RSC Advances

ROYAL SOCIETY
OF CHEMISTRY

www.rsc.org/advances

Defect-induced metallic-to-semiconducting transition in multilayer graphene

Kaliannan Thiyagarajan[a], Antony Ananth[c], Balasubramaniam Saravanakumar[a],

Young Sun Mok[c], Sang-Jae Kim[a,b*]

[a] Nanomaterials and system Lab, Department of Mechatronics Engineering, Jeju National

University, Jeju 690-756, Republic of Korea

[b] School of Material Science and Engineering, Georgia Institute of Technology, Atlanta,

Georgia 30332-0245, United States

[c] Plasma Applications laboratory, Department of Chemical and Biological Engineering,

Jeju National University, Jeju 690-756, Republic of Korea

ABSTRACT

We investigate the electrical transport properties of multilayer graphene (MLG) following irradiation with Ar plasma. The plasma induces defects, including vacancies, voids, and nanoholes, which altered the resistance of the MLG. The resulting defect-rich MLG device exhibits an asymmetric ambipolar behavior, with strong p-doping effect, which considerably deteriorates the electron conductivity, implies the defect generation on the MLG surface. The pristine MLG was metallic; however, the resulting defect-rich MLG following plasma treatment exhibited a semiconductor-like temperature dependence of the resistance. Thus, MLG with morphological disorder exhibits a metallic-to-semiconductor transition in the resistance as a function of temperature.

[*]Corresponding author,

Email: kimsangj@jejunu.ac.kr; sang.kim@mse.gatech.edu

Phone: 0082 – 64 - 754-3715; fax: 0082-64-756-3886;

1. Introduction

In recent years, researchers are very keen to modify the properties of graphene, owing to its potential applications in various fields.[1-6,] Defect engineering is one of the way to manipulate the electrical, chemical, and magnetic properties of graphene. Defects are typically viewed as imperfections in material, which may significantly degrade the material properties (physical, chemical and electrical). However, nanoscale or nanosize defects in the graphene surface could be extremely useful, if they engender a novel, ground-breaking applications.[7] Ion irradiation (Ga^+ and Ar^+),[8, 9] collision cascade,[10] and plasma irradiation[11-13] are the methods commonly used; to induce surface defects in solid materials.[10] Plasma irradiation on graphene surface may lead to forms the different types of defects: (i) structural (sp^2-like), (ii) topological (sp^2-like) (iii) doping/functionalization and impurity (sp^2- and sp^3-like), and (iv) graphene islands or vacancies/edge type defects (non-sp^2-like),[7, 14–16] which significantly affect the electrical properties of the graphene.

The properties of the ideal defect-free graphene are strongly dependent on the thickness (i.e., the number of layers), which exhibits semiconducting to metallic transition in electrical transport measurement.[17] Single layer graphene has a zero band gap,[18] while bilayer graphene exhibits a tunable band gap.[19] Bernal (ABA)-stacked trilayer graphene is semi-metallic,[20] but trilayer graphene with a Rhombohedral (ABC)-stacking is an insulator with an intrinsic (spontaneous) band gap of ~6 meV.[21] However, the band overlaps in multilayer graphene (MLG) result in metallic behavior. Bala Kumar *et al*.[22] observed a semiconducting-to-metallic transition in armchair graphene nanoribbons when varying an externally applied transverse electric field.

Here, we investigate the resistive response of the pristine and defected MLG. Here the defect was induced by the plasma irradiation, when the plasma species strike the pristine-MLG lattice, induces different types of defects, includes vacancies, voids, and nanometer-scale holes, which alters the device resistance. The morphological disorder in MLG leads to a metallic-to-semiconducting (M-SC) transition in the resistance as a function of temperature $R(T)$.

2. Experimental section

The micromechanical cleavage method was used to form multilayer graphene from highly oriented pyrolytic graphite (HOPG) via mechanical exfoliation, and the resulting MLG flakes were transferred to an SiO_2/Si substrate. Optical microscope (OM) was used to locate the MLG flake, and the color contrast method was used to determine the boundaries.[23] Atomic force microscopy (AFM) and micro Raman spectroscopy were used to characterize the thickness of the flakes. Electrodes were patterned using a conventional photolithography, a 100 nm-thick gold (Au) layer was deposited by thermal evaporation, and the electrodes were defined using lift-off. Details of the lithographic process and the method used to determine the thickness of the layers are described in Ref.[17] (see Fig. S1 in the Supplementary Information). The MLG devices were annealed at 250°C in an Ar/H_2 atmosphere for 30 min to improve the adhesion of the gold electrodes to the graphene flakes and to remove the residual resist. Prior to plasma exposure, the electrodes were covered using a thin layer of epoxy resin, and dried at 150°C for 30 min in the air to prevent oxidization and damage to the electrodes.

The MLG device was then exposed to a custom-made atmospheric plasma reactor in Ar atmosphere with a flow rate of 60 sccm at a pressure of ~1 Torr for 10 min. The plasma irradiation induces surface defects and also generates nanoholes which is schematically shown in

Fig. 1a. We compare the OM image of the same MLG before and after plasma irradiation (see Fig. 1b and 1c), but there are no obvious changes observed. Longer plasma irradiation on graphene surface leads to significant defect generation and then to etching, which causes the sample thickness, in case of MLG the thickness variation is in the sub nanometer range see Fig.S2. To characterize the defects nature and its type, we carry out Raman spectroscopy measurements, using Horiba Jobin Yvon, LabRAM HR800, where the spot size of the laser is ~1 μm for 100x objective, and the power of 514 nm Ar^+ ion laser is 10mW, but only 10% was applied to avoid heating. Nanoview surface profile analysis (Nano System Co., Ltd.) was employed to visualize the surface defects. Field-emission scanning electron microscopy (FESEM) (JEOL, JSM-6700F) was used to characterize the structural changes in the plasma-treated samples. Room-temperature electrical measurements were carried out using a semiconductor parameter analyzer (Agilent, B 1500A). Low-temperature electrical transport measurements of the devices were performed using a closed-cycle refrigerator system (CKW-21, Sumitomo-Japan), allowing us to characterize the devices at temperatures in the range of 15–300 K using a Keithley 2182A nanovoltmeter and a Keithley 2400 source meter.

3. Results and discussion

Defect-rich graphene sheets, exhibits significant differences in their physicochemical properties, when compared to the pristine graphene.[7] The thickness of the flakes and the process parameters determines the defect density. Plasma irradiation induces a number of different types of defects on the surface of the MLG; [14,15] however, defects are typically generated from existing Stone–Thrower–Wales (STW) defects. The MLG sheets react with the Ar plasma species to form

a defect (i.e., a vacancy or nano-scale hole); these defects result in a change in the electrical resistance of the MLG.

The defect nature of the MLG devices was characterized using Raman spectroscopy. Fig. 2 shows the first-order and second-order Raman spectra of pristine-MLG and plasma-irradiated MLG (p-MLG), here the spectrum was normalized to show the appearance of defect related peaks clearly. The Raman spectrum of the pristine-MLG exhibited graphitic (G and 2D) peaks, and a disorder D peak was not observed, which indicates the crystalline nature of MLG. In contrast, the p-MLG exhibited graphitic peaks as well as defect-associated (D, D′ and D+G) peaks. Here, the Raman-inactive D peak, which was attributed to the A1g symmetry of phonons near the K-zone, became active due to the presence of structural disorder. [24,25] The defect-related D peak appeared at 1364 cm^{-1}, and another disorder-related (D′) peak appeared at 1628 cm^{-1}, which was attributed to intravalley phonons.[26] An additional peak appeared at 2958 cm^{-1}, which was attributed to D+G overtones. The existence of these defect-related peaks, and the increase in the full-width at half-maximum (FWHM) of the G and 2D peaks suggests the formation of structural disorder in the p-MLG. The concentration of the defects is given by the ratio of $I_{(D)}$ /$I_{(G)}$, and the defect type is given by the $I_{(D)}/I_{(D')}$ ratio. In our case, the defect concentration is 0.431 and the, $I_{(D)}$ /$I_{(D')}$ value is 3.26. These values suggest that the defects were due to vacancies, voids, and nano-scale holes.[27] The flake height variation in MLG affects the defect size distribution. The step and the edges of the flake as the more defects and the size of the nanohole also huge due to the long time plasma irradiation on the Stone–Thrower–Wales (STW) defect sites see Fig. S3. The density and nature of these defects strongly depend on the production and processing techniques, and we may expect some sample-to-sample variation in the graphene specimens.

The obtained Raman spectrum (Fig.2) suggests that the generated defects are holes, here we used FESEM analysis to visualize the defect. Fig. 3a–d shows FESEM images of the p-MLG in different magnification on a silicon wafer following Ar plasma treatment. Nanoholes and vacancies are clearly visible; the size of the nanoholes varied in the range 100–500 nm. The FESEM images could not resolve the point-like defects, which were present all over the surface. In contrast, the pristine-MLG exhibited a smooth surface (see Fig. S4 in the Supplementary Information). Defects in p-MLG lead to an increase in the surface area, and the disorder at the surface results in localized regions of amorphous carbon atoms.[28]

To further corroborate the Raman, FESEM results and to measure the depth of the defect, we employed 3D nano profiler analysis. Fig. 4a and 4b show images of the p-MLG, and the corresponding line profiles are shown in Fig. 4c and d. The 3D view shown in Fig. 4b reveals that the entire surface of the MLG was affected by plasma irradiation. The roughness of the surface significantly increased following the plasma treatment, and served as clear evidence of the presence of defects. The plasma-induced nanoholes had various depths (see Fig. 4c and 4d); this variation may be promoted by the presence of ultra-small defects, such as STW defects or corrugated surfaces,[29] and then the synergistic effect of plasma carries the process further.[30] A high-magnification, 3D view of a single nanohole is shown in Fig. 4e; the width was ~ 4 μm and the depth was ~ 8.2 nm. In order to check the width of the nanohole with respect to its depth (height), we have processed the image in Fig. 4e using image-processing software (SPIP 6.2.5), and the resulting image is shown in Fig. 4f, here the different color indicates that the width decreases when the depth of the nanoholes increases. These surface defects and nanoholes are the conductivity causing factors of the p-MLG.

The plasma induced defect alters the electrical transport properties of the device. To investigate that we measured the current–voltage (*I–V*) characteristics of the MLG sample at room temperature (Fig. 5a). The linear *I–V* response of pristine-MLG indicates the formation of Ohmic contacts between the Au electrodes and the MLG channel. The large current at an applied bias of 5 V shows that the resistance of the pristine-MLG was small. When the MLG was irradiated with Ar plasma for 10 min, the synergistic effect of the plasma species, including ions, electrons, photons, and metastable neutral atoms[30] struck the graphene lattice, which broke the π–π bonds, allowing some carbon atoms to detach, producing the nanoscale holes. The resulting p-MLG exhibited nonlinear *I–V* curves, as shown in Fig. 5a, with a drop in the current value of three orders of magnitude.

To elucidate the electrical properties of this p-MLG, we fabricate field-effect transistor (FET) with back-gate configuration (see the inset of Fig. 5b) and measured the transfer characteristics at room temperature. Fig. 5b shows the resistance (R) as a function of back-gate voltage (V_{bg}), where the p-MLG device exhibits asymmetric ambipolar behavior and the Dirac point (maximum resistance, V_{DP}) is located around 39 V, whereas the ambipolar characteristic is absence in pristine-MLG device (data not shown). This p-type behavior of the p-MLG device clearly suggest that the plasma irradiation leads to increase p-doping effect which deteriorates the electron conductivity (adsorbance of water and oxygen molecules) [31] and introduce an asymmetry between electron and hole transport [32] (semiconducting behavior), which leads to increase the device resistance.

It's necessary to identify the functional group involved in the p-doping effect of p-MLG. We performed an XPS analysis to investigate the p-doping effect, Fig. 5c and d, shows the C1s

core level spectra corresponds to pristine and p-MLG devices, where the pristine-MLG exhibit two components, the peak at 284.6 eV is belong to sp^2 carbon (C=C/C–C) bonds and the other peak at 285.8 eV was assigned to C–O (non-covalent) bond this may arise during device fabrication.[33] The C1s spectra of p-MLG (Fig.5d) also shows a sp^2 carbon (C=C/C–C) peak at 284.6 eV, which significantly differs from pristine-MLG when the peak emerges at 285.0 eV which is attributed to the sp^3carbon due to the removal of carbon atoms (amorphous defect generation), [34, 35] leads to deteriorating the electrical conductivity. The peak corresponds to C–O (286.3 eV) which has the possibility of forming epoxy and a hydroxyl group. For epoxy formation, one O atom bridging over two neighboring carbon atoms, because of the O2p orbital strongly hybridizes with extended π π* bands in graphene it changes the carbon planer (sp^2) hybridization to distorted sp^3 hybridization.[36] In case of hydroxyl formation the O atom is on top of a carbon with C–O bond nearly perpendicular to the graphene plane, which causes the change in carbon hybridization from sp^2 to sp^3 by forming a strong covalent bond between C and O. The peak at 288.5 eV ascribed to the formation of carbonyl bonds (C=O), [14] this may be a ketone. Soon or after defect generation, oxygen molecules from the atmosphere reacts with defected p-MLG surface and forms hydroxyl, epoxy and carbonyl functional groups, which increased the device resistance considerably.

To further evaluate this resistance changing behavior of p-MLG, we measured the temperature dependence of the resistance (R (T)) measured based on the with four probe method. Fig. 6a and b shows the R (T) behavior of the pristine and p-MLG device, with the sample thickness of ~21 and ~35 respectively. Where the resistance of the pristine-MLG decreases, when the temperature decreases (metallic nature), which was attributed to the overlapping bands, different stacking sequences, splitting of the π-band, and interlayer hopping of the charge

carriers.[17, 37, 38] In contrast, the temperature dependence of p-MLG was similar to that of a semiconductor, where the resistance decreased with increasing temperature. This metallic to semiconducting like behavior exhibits even with the device irradiated over 8 min of time, but the resistance variation is very small (see Fig. S5) when compared to the device presented in Fig. 6a and b. This semiconducting behavior overwhelms due to the formation of various types of defect, such as point defects, vacancies, and nanoholes.[2] The sharp D-peak intensity, splitting of the G-peak, increment in the G-peak intensity (Raman spectra, Fig. 2), visualization of the defects, nanoholes in the 3D nanoprofiler analysis (Fig. 4b) indicates the formation of a large defect density and a drop in crystallinity (increment in the sp^2/sp^3 ratio), which significantly increases the resistance of the p-MLG.[2, 39]

Fig. 6c shows the current-biased, *I–V* characteristic of the pristine and p-MLG device at 150 K. We can clearly see a linear to non-linear transition in the *I–V* curves after the pristine-MLG was exposed to the Ar plasma. Similar behavior was observed at all temperatures (see Fig. 6d). The temperature dependence of the resistance of the pristine and p-MLG (four samples) is shown in Fig. 6e and f. The resistance of the p-MLG increased with decreasing temperature from 300 K down to 20 K, is mainly due to the deficiency of thermal excitation and hopping of charge carriers.

Charge transport in p-MLG can be described by a combination of (i) tunneling, (ii) hopping, (iii) *c*-axis conduction across nanoholes, and (iv) percolative conduction pathways. The plasma induces stacking faults, charge transport across these stacking faults is by tunneling.[40] A reduction in the hopping current across the holes with decreasing temperature due to the reduction in thermal excitation leads to an increase in the resistance of the p-MLG. In

defect-free graphene, current flows across the graphene channel in the *ab*-plane, and *c*-axis charge transport is not significant; however, *c*-axis conduction becomes more significant here due to the presence of the nanoholes in the p-MLG. The charges flow in the *ab*-plane, [38] but diverge at the walls of the nanoholes.[13] With a sufficiently large defect density, charge transport in p-MLG follows percolative conduction pathways. [2, 13] This defect induced M-SC transition in MLG will be useful in nonlinear device applications.

4. Conclusions

We have investigated the change in the electrical properties of MLG following exposure to an Ar plasma. The plasma induces vacancies, voids, and nanoholes on MLG, which resulted in an increase in the device resistance. The p-MLG exhibited a semiconductor-like temperature dependence of the resistance, where the electrical conduction is the combination of tunneling, hopping, and *c*-axis conduction between graphene sheets at nanoholes and, in regions of large defect densities, charge transport was via percolation. This defect-induced M-SC transition in MLG has potential applications in advanced nonlinear devices.

Supplementary Information.

The thickness approximation, atomic force microscopy, Raman spectroscopy analysis of the pristine and defected MLG and FESEM analysis of pristine MLG are available in the online version.

Acknowledgements

Notes and References

[1] P. Sun, M. Zhu, K. Wang, M. Zhong, J. Wei, D. Wu, Y, Cheng, and H. Zhu, Appl Phys Lett., 2012, 101, 053107.

[2] E. X. Zhang, A. K. M. Newaz, B. Wang, C. X. Zhang, D. M. Fleetwood, K. I. Bolotin, R. D. Schrimpf, S. T. Pantelides, and M. L. Alles, *Appl. Phys. Lett.,* 2012**, 101***,* 121601.

[3] Yi-T. Liu, M. Dang, Xu-M. Xie, Z-F. Wang and X-Y. Ye *J. Mater. Chem.,* 2011, **21,** 18723–18729.

[4] Yi-T. Liu, X-D. Zhu, Z-Q. Duan and Xu-M. Xie *Chem. Commun.,* 2013,**49,** 10305–10307

[5] Yi-T. Liu, Q-P. Feng, Xu-M. Xie, and X-Y. Ye, *Carbon* 2011, **49,** 3371–3375.

[6] Yi-T. Liu, Xu-M. Xie, and X-Y. Ye *Carbon* 2011, **49,** 3529–3537.

[7] H. Terrones, R. Lv, M. Terrones, and M. S. Dresselhaus, *Rep. Prog. Phys.,* 2012, **75,** 062501.

[8] S. H. Al-Harthi, A. Kara`a, T. Hysen, M. Elzain, A. T. Al-Hinai, and M. T. Z. Myint, *Appl. Phys. Lett.,* 2012, **101,** 213107.

[9] Y.B. Zhou, Z. M. Liao, Y. F. Wang, G. S. Duesberg, J. Xu, Q. Fu, X. S. Wu, and D. P. Yu, *J Chem Phys.,* 2010, **133,** 2347031.

[10] K. Kitagawa, K. Yamakawa, H. Fukushima, T. Yoshiie, Y. Hayashi, H. Yoshida, Y. Shimomura, and M. Kiritani, *J. Nucl. Mater.,* 1985, **133–134***,* 395–399.

[11] Y. C. Cheng, T. P. Kaloni, Z. Y. Zhu, and U. Schwingenschlögl, *Appl. Phys. Lett.,* 2012, **101**, 073110.

[12] Z. Fang, Y. Wang, Z. Liu, A. Schlather, P. M. Ajayan, F. H. L, Koppens, P. Nordlander, and N. J. Halas, *ACS Nano,* 2012**, 6,** 10222–10228.

[13] K. Thiyagarajan, A. Ananth, B. Saravanakumar, Y. S. Mok and S. J. Kim, *Carbon,* 2014, **73***,* 25–33.

[14] A. Nourbakhsh, M. Cantoro, A. V. Klekachev, G. Pourtois, T. Vosch, J. Hofkens, M. H. van der Veen, M. M. Heyns, S. De Gendt, and B. F. Sels, *J Phys Chem C,* 2011, **115***,* 16619–16624.

[15] A. K. Singh, E. S. Penev, and B. I. Yakobson, *ACS Nano,* 2010, **4,** 3510–3514.

[16] S.O. Woo, and W. Teizer, *Appl Phys Lett.,* 2013, **103,** 041603.

[17] K. Thiyagarajan, B. Saravanakumar, R. Mohan, and S. J. Kim, *Sci Adv Mater.,* 2013, **5,** 542–548.

[18] A. K. Geim, *Science,* 2009, **324,** 1530–1534.

[19] Yacoby, *Nature Phy.,* 2011, **7,** 925–926.

[20] M. F. Craciuna, S. Russob, M. Yamamotoc, and S. Taruchac, *Nano Today,* 2011, **6,** 42–60.

[21] W. Bao, L. Jing, Jr. Velasco, Y. Lee, G.Liu, D. Tran, B. Standley, M. Aykol, S. B. Cronin, D. Smirnov, M. Koshino, E. McCann, M. Bockrath, and C. N. Lau, *Nature Phy.,* 2011, **7,** 948–952.

[22] S. Bala Kumar, and J. Guo, *Appl. Phys. Lett.,* 2011, **98,** 263105.

[23] Z. H. Ni, H. M. Wang, J. Kasim, H. M. Fan, T. Yu, Y. H. Wu, Y. P. Feng, and Z. X. Shen, *Nano Lett.,* 2007, **7,** 2758–2763.

[24] C. Thomsen, and S. Reich, *Phys. Rev. Lett.,* 2000, 85, 5214–5217.

[25] R. Rozada, P. Solıs-Fernandez, J.I. Paredes, A. Martınez-Alonso, H. Ago, and J.M.D. Tascon *Carbon* 2014, **79,** 664–669.

[26] L.G. Cancado, M. A. Pimenta, B. R. A. Neves, M. S. S. Dantas, and A. Jorio *PRL* 2004, **93,** 247401-1247401-4.

[27] A. Eckmann, A. Felten, A. Mishchenko, L. Britnell, R. Krupke, K. S. Novoselov, and C. Casiraghi, *Nano Lett.,* 2012, **12,** 3925–3930.

[28] P. Me´linon, A. Hannour, L. Bardotti, B. Pre´vel, J. Gierak, E. Bourhis, G. Faini, and B. Canut, *Nanotechnology,* 2008, **19,** 235305.

[29] B. Prével, J. M. Benoit, L. Bardotti, P. Mélinon, A. Ouerghi, D. Lucot, E. Bourhis, and J.Gierak, *Appl Phys Lett.,* 2011, **99,** 083116.

[30] B. Rousseau, H. E. Szwarckopf, A. L. Thomann, and S. P. Brault, *Appl. Phys. A,* 2003, **77,** 591–597.

[31] T. Feng, D. Xie, H. Zhao, G. Li, J. Xu, T. Ren, and H.Zhu, *Appl. Phys. Lett.,* 2013, **103,** 193502.

[32] A. Jacobsen, F. M. Koehler, W. J. Stark, and K. Ensslin, *New Journal of Physics,* 2010, **12,** 125007.

[33] K. Choi, J. Lim, J. R. Rani, H. S. Yoon, J. Oh, T. Hong, T. Ha, B. C. Park, K.I. Sim, S. C. Jun, and J. H. Kim *Appl. Phys. Lett.* 2013, **102,** 131901.

[34] S. Yeo, C. Choi, C. W. Jang, S. Lee, and Y. M. Jhon, *Appl Phys Lett.,* 2013, **102,** 073108.

[35] Y. Su, S. Pei, J. Du, W. B. Liu, C. Liu, and H. M. Cheng, *Carbon,* 2013, **53,** 4–10.

[36] J. A. Yan, and M. Y. Chou, *Phy. Rev. B,* 2010, *82*, 125403.

[37] T. Ohta, A. Bostwick, J. L. McChesney, T. Seyller, K. Horn, and E. Rotenberg, *Phys. Rev. Lett.,* 2007, **98,** 206802.

[38] G. Venugopal, M. H. Jung, M. Suemitsu, and S. J. Kim, *Carbon,* 2011, **49,** 2766–2772.

[39] N. Leconte, J. Moser, P. Ordejon, H. Tao, A. Lherbier, A. Bachtold, F. Alsina, C. M. Sotomayor-Torres, J. C. Charlier, and S. Roche, *ACS Nano,* 2010, **4,** 4033–4038.

[40] S. Ono, *J. Phys. Soc. Jpn.,* 1976**, 40,** 498–504.

Figure captions

Fig. 1. (a) Schematic of diagram nanoholes multilayer graphene device. Optical microscopy image of MLG (b) before and (c) after plasma irradiation.

Fig. 2. Micro-Raman spectrum (λ = 532 nm) of the pristine and plasma-irradiated devices. The inset at the top-left shows an optical microscopy image, and the inset at the top-right shows a FESEM image of a typical device.

Fig. 3. FESEM image of p-MLG: (a) surface with different stack heights, (b) an enlarged view of the stack, (c) nanoholes of various sizes, and (d) a magnified image of a single nanohole.

Fig. 4. Surface profile analysis. (a) Two-dimensional image of p-MLG; here, the numbers 1 to 6 indicate the plasma-generated nanoholes. (b) 3D image of the data shown in (a). Line profiles of (c) the *x*- and (d) the *y*-axis of the data shown in (a). (e) High-magnification image of a single nanohole (numbered 4 in (a) and (b)). (f) Processed 3D image of the data shown in (e).

Fig. 5. (a) Voltage-biased *I–V* curves of the pristine-MLG and p-MLG at room temperature, (b) Transfer characteristics of the p-MLG Field effect transistor device at the drain source voltage of 500 mV, Inset is the schematic of the p-MLG FET device. (c) and (d) C1s high-resolution XPS

spectra of the pristine and p-MLG respectively. (Note that the spectra were deconvoluted using the Shirley method of background removal).

Fig. 6. (a) and (b) Temperature dependence of the resistance R (T) of pristine and p-MLG device with the sample thickness of ~21 and 35 nm device respectively.(c) Current-biased, $I–V$ curves of the pristine and p-MLG device at 150 K. (d) Current biased temperature dependent $I-V$ characteristic of p-MLG at various temperature. (e) and (f) Temperature dependent resistance change of four different devices at room temperature (300 K) and low temperature (20 K) respectively (green color (dash dot dot) line is the guideline to the eye).

Supplementary Information:

Fig. S1. AFM analysis: (a) 2D image of pristine-MLG and (b) 3D image of (a). (c) The line profile image corresponding to the x-axis of (a) which shows the thickness of ~ 35 nm.

Fig. S2. (a) The two-dimensional AFM image of the p-MLG (b) and (c) Line profile image corresponding to the x-axis of (a) before plasma irradiation (pristine-MLG), after plasma irradiation (p-MLG) respectively.

Fig. S3 - Micro-Raman spectrum of the pristine (red) and p-MLG device at different places holes (blue) and steps (green).

Fig. S4. FESEM image of pristine-MLG (a) Surface of the pristine-MLG (b) Magnified image of the marked (yellow color) area of the pristine-MLG (a) shows the smooth surface.

Fig. S5- Temperature dependence of the resistance $R (T)$ of pristine and p-MLG device.

Figures
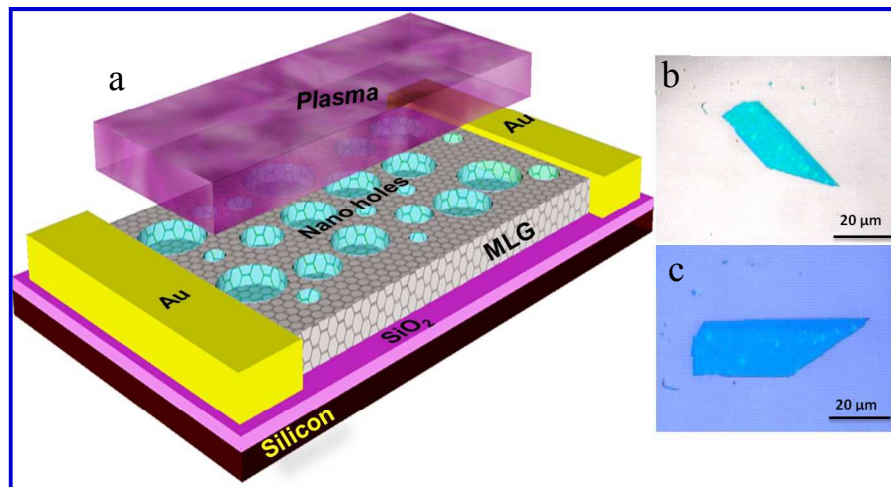
Fig.1
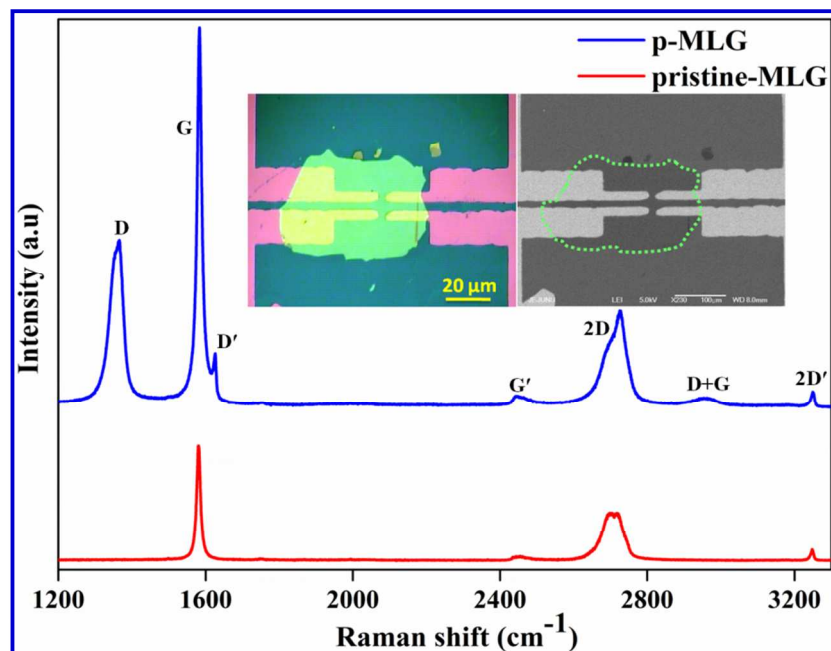
Fig.2
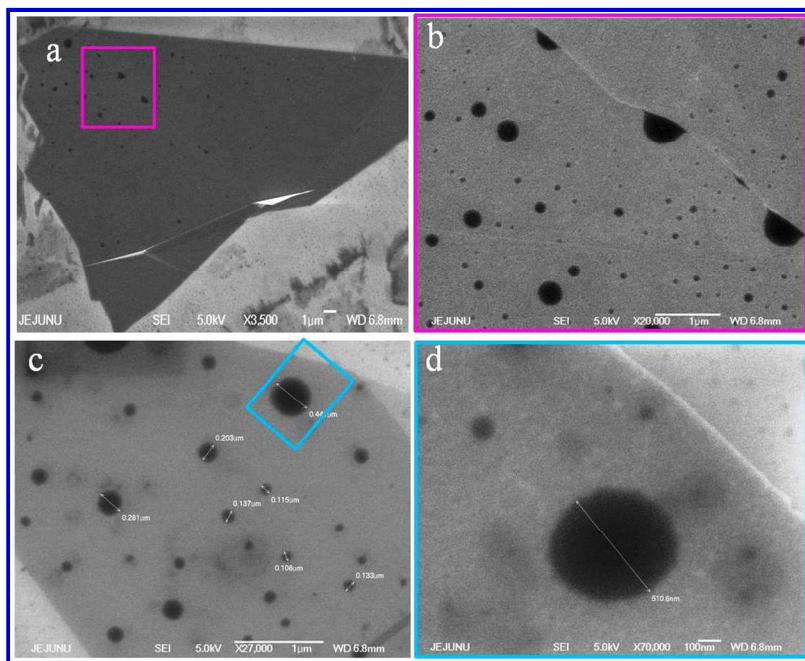
Fig.3
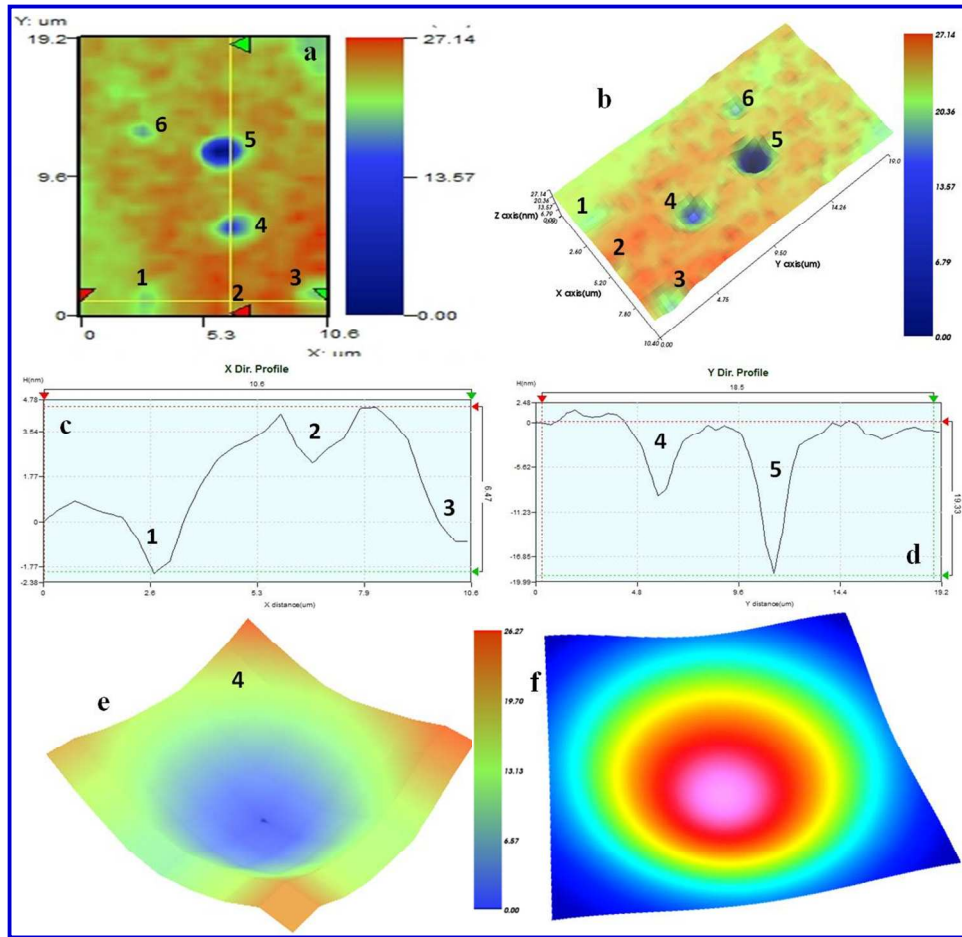
Fig.4
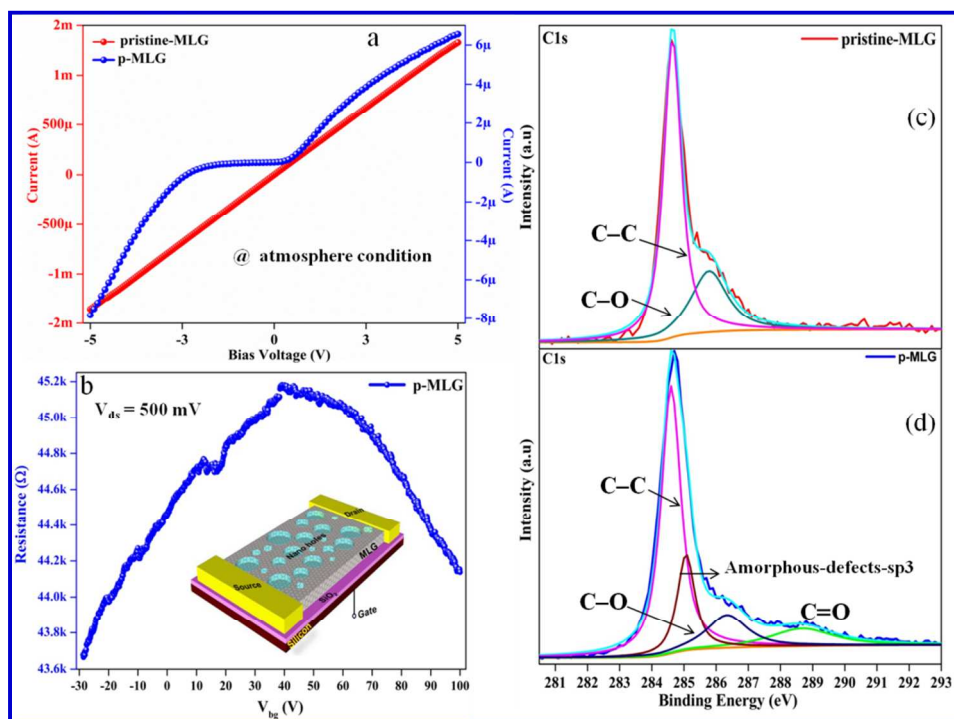
Fig.5
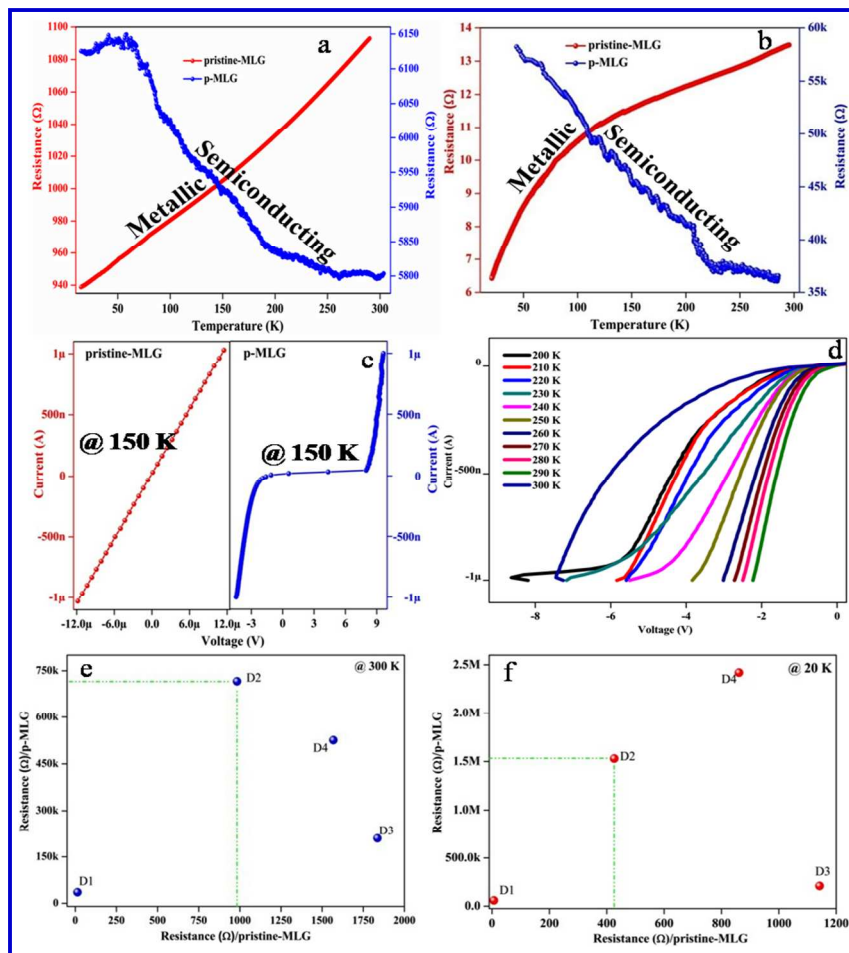
Fig.6
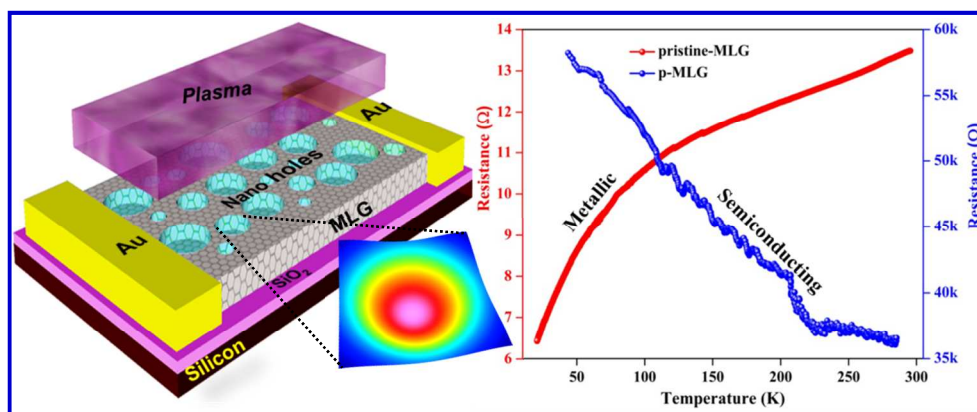
TOC Figure

The morphological disorder in multilayer graphene behaves like a semiconductor at low temperature.